MATERIALS CHEMISTRY FRONTIERS

RESEARCH ARTICLE

View Article Online
View Journal | View Issue

Cite this: *Mater. Chem. Front.*, 2021, **5**, 5841

Photoactive conjugated polymer/graphdiyne nanocatalyst for CO_2 reduction to CO in living cells for hypoxia tumor treatment†

Endong Zhang,[ab] Zicheng Zuo,[a] Wen Yu,[ab] Hao Zhao,[ab] Shengpeng Xia,[ab] Yiming Huang,[a] Fengting Lv,[a] Libing Liu,[a] Yuliang Li*[a] and Shu Wang*[a]

Received 9th May 2021,
Accepted 13th June 2021

DOI: 10.1039/d1qm00677k

rsc.li/frontiers-materials

Carbon monoxide (CO) gas therapy has grown to be an emerging tumor therapy strategy to avoid the low treatment efficiency of photodynamic therapy (PDT) caused by the hypoxia tumor microenvironment. However, intracellular *in situ* generation of CO for hypoxia tumor treatment remains challenging. Herein, photoactive conjugated polymer/graphdiyne nanocatalyst (CP@GDY/DSPE-PEG) was constructed to *in situ* reduce endogenous carbon dioxide (CO_2) into CO for hypoxia tumor therapy. Under light irradiation, the CO production rates of PFP@GDY/DSPE-PEG and PBF@GDY/DSPE-PEG reached 23 μmol h^{-1} $gmat^{-1}$ and 31 μmol h^{-1} $gmat^{-1}$ respectively, which can significantly affect mitochondrial respiration, leading to cancer cell apoptosis. Thus, the therapeutic effect of catalysis from metabolic CO_2 into CO therapy under hypoxia conditions was achieved. This work provides a conjugated polymer/graphdiyne nanocatalyst to *in situ* generate CO for hypoxia tumor treatment.

Cancer, as one of the high fatality diseases, has threatened global public health.[1–6] A major obstacle to cancer therapy is the extreme hypoxia tumor microenvironment, which is usually caused by the rapid proliferation of tumor cells and enormous oxygen (O_2) consumption.[2–14] Relatively low O_2 concentration limits photodynamic strategy for long-term cancer therapy in hypoxia conditions.[15–18] Development of new therapeutic methods or agents for hypoxia cancer therapy is still highly required.

Carbon monoxide (CO), as one of the therapeutic gas molecules, has been utilized for hypoxia tumor treatment in an O_2-free manner.[19] CO can interfere with the second stage of mitochondrial respiration and further affects the balance of ATP production, finally inducing cell apoptosis.[20] Recently, CO releasing molecules (CORMs) have been prepared as nanoparticles by coordinating CO molecules with transition metals for intracellular CO delivery.[21] The release of CO could be spatiotemporally triggered by a variety of external stimuli.[22–26] The disadvantages of deficient delivery capacity, ineffective delivery efficiency, and uncontrollable release amount of CO still severely limit the development of CO therapy for tumor treatment.

Alternatively, we aim to develop biocompatible materials that can convert metabolic CO_2 into CO *in situ* for antitumor treatment in hypoxia conditions, which would be highly desirable for hypoxia cancer therapy. Rapid metabolism of cancer cells increases the level of respiratory metabolism of CO_2, causing higher HCO_3^- concentration in the hypoxia tumor microenvironment.[27] Combined with low O_2 level and high CO_2 level of the hypoxia condition, *in situ* photo-catalytic CO_2-to-CO conversion avoids the limitation of insufficient O_2 and continually generates therapeutic CO. Organic semiconducting materials provide promising choices for such photocatalytic applications. Conjugated polymers (CPs) have attracted much attention in biosensors, imaging, and bioelectronics due to their π-extended conjugated structure and strong light-harvesting ability.[23–25,28–30] By designing the π-conjugated backbone of the CPs, the bandgap could be variably tuned.[31–33] In comparison with organic dyes and inorganic quantum dots, CPs with high brightness, excellent photostability, and low cytotoxicity are preferred as light-sensitive molecules in a photocatalyst system. Besides, graphdiyne (GDY) is a new type of two-dimensional carbon allotrope material, in which consecutive diacetylenic triangular structure between adjacent benzene rings constitutes the basic structural unit of GDY. Owing to the highly delocalized π bonds and large specific surface area, GDY shows good electron transfer efficiency and

[a] *Beijing National Laboratory for Molecular Science, Key Laboratory of Organic Solids, Institute of Chemistry, Chinese Academy of Sciences, Beijing, 100190, China. E-mail: ylli@iccas.ac.cn, wangshu@iccas.ac.cn*

[b] *College of Chemistry, University of Chinese Academy of Sciences, Beijing 100049, China*

† Electronic supplementary information (ESI) available: Detailed experimental procedures and Fig. S1–S4. See DOI: 10.1039/d1qm00677k

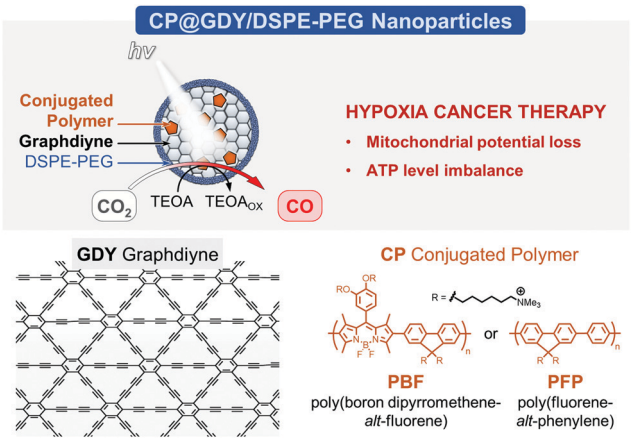

Scheme 1 . Schematic illustration of CP@GDY/DSPE-PEG nanocatalysts converting endogenous CO_2 into CO for hypoxia cancer therapy and chemical structure of graphdiyne and conjugated polymers (PFP and PBF).

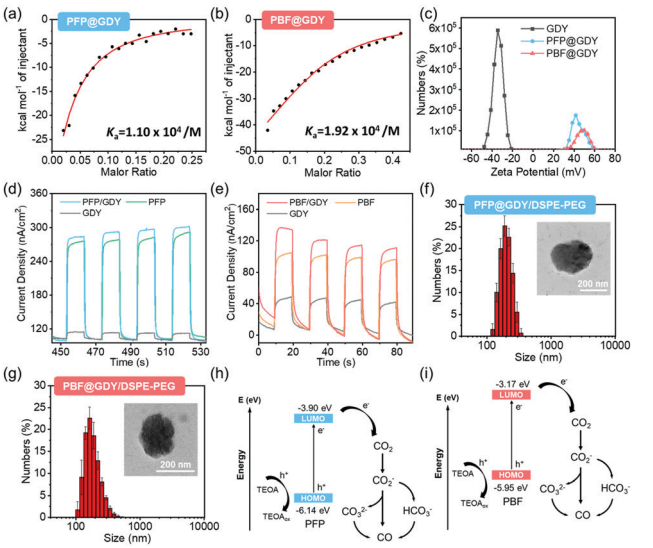

Fig. 1 Absorption and fluorescence spectra of PFP and PBF. Fitting curves of ΔH_{obs} against the GDY/CPs molar ratio by titrating GDY into PFP solutions (a) and PBF solution (b). (c) Zeta potential of GDY and CP@GDY. (d) Photocurrents of PFP, GDY, and PFP/GDY. (e) Photocurrents of PFP, GDY, and PFP/GDY. (f) Size from DLS and TEM images of PFP@GDY/DSPE-PEG. (g) Size from DLS and TEM images of PBF@GDY/DSPE-PEG. The scale bar is 200 nm. Energy levels of PFP (h) and PBF (i) for electron transfer to reduce CO_2 into CO.

adsorptive property.[34] GDY possesses a porous structure that provided a good three-dimensional substrate in catalytic gas reactions.[35,36]

In this work, water-soluble nanocatalysts (CP@GDY/DSPE-PEG) that can catalytically reduce CO_2 into CO for cancer therapy in hypoxia conditions were developed through the assembly of conjugated polymers (CPs, PFP, and PBF) with GDY by electrostatic and hydrophobic interactions. The introduction of amphiphilic DSPE-PEG2000 imparted CP@GDY with good dispersibility in an aqueous solution. The CO production rates of PFP@GDY/DSPE-PEG and PBF@GDY/DSPE-PEG respectively reached 23 μmol h^{-1} $gmat^{-1}$ and 31 μmol h^{-1} $gmat^{-1}$ under hypoxia condition. CP@GDY/DSPE-PEG could be internalized by cancer cells located in the lysosome. They catalyzed the reduction of endogenous CO_2 into CO, which affected mitochondrial respiration. Meanwhile, intracellular ATP level was changed, leading to cell apoptosis through the mitochondrial pathway (Scheme 1).

The absorption and fluorescence spectra of conjugated polymers PFP and PBF were measured and are shown in Fig. S1 (ESI†). GDY was synthesized by a Glaser coupling reaction with hexaethynylbenzene as the precursor. Quantitative interaction thermodynamic parameters of CP@GDY were calculated from the isothermal titration calorimetry (ITC) fitting curves (Fig. 1a and b). Upon dropwise addition of GDY suspension into CPs aqueous solution, the initial enthalpy change (ΔH_{obs}) is negative, indicating that the interaction of GDY and CPs is an exothermic process. With the addition of GDY, ΔHobs decreased and approached zero, implying that the binding process gradually approached saturation. The ΔH_{obs} and binding constant (K) indicate that the assembly between CPs and GDY is dominated by electrostatic interactions. The binding constants (K) of GDY with PFP and PBF are calculated to be 1.10×10^4 M^{-1} and 1.92×10^4 M^{-1}, respectively. As shown in Fig. 1c, the zeta potential of GDY was measured to be -34.2 ± 0.33 mV, suggesting the negative charge characteristic of GDY. Upon addition of the same equivalent CPs to form the CP@GDY composite, the zeta potential of CP@GDY changed to 44.6 ± 0.72 mV (PFP@GDY) and 43.5 ± 0.60 mV (PBF@GDY), respectively, due to the quaternary amine group in the side chain of CPs. The thermodynamic and zeta potential results illustrated that the interactions of GDY with CPs were dominated by electrostatic interactions. As displayed in Fig. 1d and e, compared to CPs, the introduction of GDY promoted the photocurrent of CPs, which exhibited the photogenerated electron ability of CP@GDY. To obtain a stable nanocatalyst in aqueous solution, amphiphilic DSPE-PEG2000 was utilized to realize CP@GDY/DSPE-PEG by hydrophobic interactions, which was well dispersed in the aqueous solution. The sizes of PFP@GDY/DSPE-PEG and PBF@GDY/DSPE-PEG were measured to be 187.5 ± 4.2 nm and 202.0 ± 5.6 nm, respectively from dynamic light scattering (DLS), which is well consistent with transmission electron microscopy results (TEM) (Fig. 1f and g). To ensure the feasibility of CP@GDY to invert CO_2, ultraviolet photoelectron spectroscopy (UPS) was utilized for theoretically calculating the highest occupied molecular orbital (HOMO) of CPs (Fig. S2a and b, ESI†). As shown in Fig. 1h and i, under light irradiation, the CPs produced the holes and electrons, and the electron transited into the lowest unoccupied molecular orbital (LUMO) following the reduction of CO_2 into CO. Due to the large specific surface area and good electron transfer efficiency, GDY provided a three-dimensional substrate that promoted the catalytic reaction.

To verify the catalytic CO generation ability of CP@GDY/DSPE-PEG, the amount of CO was measured using gas chromatography (GC) and compared with the CO standard curve (Fig. S3, ESI†). As shown in Fig. 2a, the CO production rates of PFP@GDY/DSPE-PEG and PBF@GDY/DSPE-PEG were

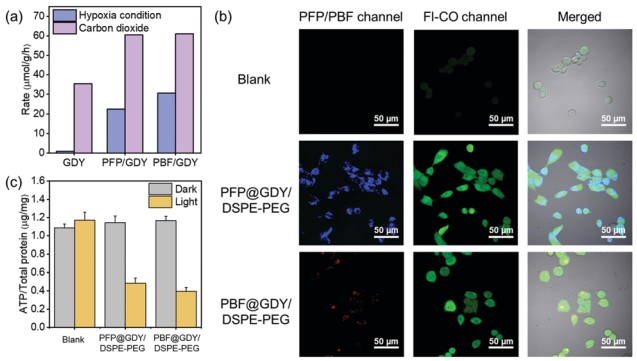

Fig. 2 (a) CO production rates for PFP@GDY/DSPE-PEG and PBF@GDY/DSPE-PEG in hypoxia condition and pure carbon dioxide. (b) CLSM image of 4T1 cells with treatment of CP@GDY/DSPE-PEG in the presence of Fl-CO after irradiation. The scale bar is 50 μm. (c) ATP level of 4T1 cells measured using the ATP kit assay.

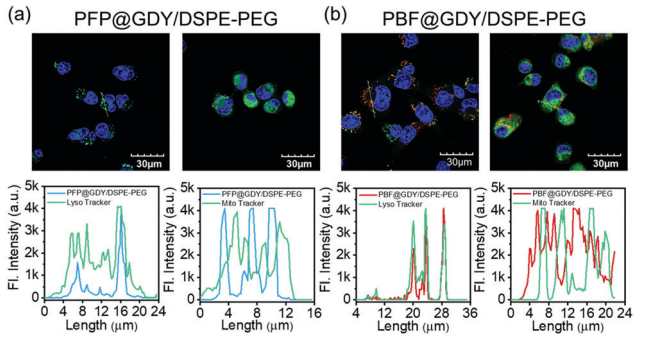

Fig. 3 Co-localization analysis of PFP@GDY/DSPE-PEG (a), and PBF@GDY/DSPE-PEG (b) in 4T1 cells. Scale bar is 30 μm.

23 μmol h^{-1} $gmat^{-1}$ and 31 μmol h^{-1} $gmat^{-1}$ in simulative hypoxia atmosphere (1% O_2), respectively, which were much higher than that of GDY without modification by CPs. To test the CO production in the cells, the CO probe (Fl-CO) was synthesized according to a previous report.[14] In the presence of CO, the dipropenyl carbonate group was removed by Tsu-ji-Trost reaction, followed by the release of fluorescent molecules. The probe had selectivity for CO and did not interfere with other ROS, reactive nitrogen species, and reactive sulfur. As shown in Fig. S4 (ESI†), with the gradual addition of CO into the Fl-CO solution, the fluorescence intensity at 520 nm increased dramatically, implying the fluorescent response to CO. The cytotoxicity of CP@GDY/DSPE-PEG and triethanolamine (TEOA) were investigated *via* a standard MTT assay (Fig. S5, ESI†). The CP@GDY/DSPE-PEG was incubated with 4T1 cells for 12 h to ensure complete entry into the cells. The cancer cells were incubated under hypoxia conditions for another 6 h, consuming the O_2 at a hypoxia level. As shown in Fig. 2b, in the presence of TEOA, strong fluorescence was observed for the 4T1 cells treated with CP@GDY/DSPE-PEG under visible light irradiation. This result indicated that CP@GDY/DSPE-PEG could capture endogenous CO_2 and photo-catalytically reduce it into CO. It was reported that CO could enhance intracellular adenosine triphosphate (ATP), thus the ATP level was measured and is shown in Fig. 2c. The result was contrary to conjecture and showed declining ATP levels when treated with CP@GDY/DSPE-PEG. We speculated that there was 1% O_2 providing CP@GDY/DSPE-PEG to produce ROS under hypoxia conditions, which disturbed the intracellular level.

Prior to studying the anticancer activity, the distribution of CP@GDY/DSPE-PEG inside 4T1 cells was investigated by confocal laser scanning microscopy (CLSM). As shown in Fig. 3a and b, the fluorescence of PFP@GDY/DSPE-PEG (blue emission) and PBF@GDY/DSPE-PEG (red emission) merged well with that of the lysosomal tracker but not for the mitochondrial tracker, indicating that the nanocatalyst is mainly located at the lysosome. To confirm that CP@GDY/DSPE-PEG could catalytically reduce CO_2 into CO for hypoxia cancer therapy, the cell viability with irradiation treatment was studied using the MTT assay. As shown in Fig. 4a and b, CP@GDY/DSPE-PEG showed obvious anticancer influence on the viability of 4T1 cells with increasing concentration of the nanocatalyst. In comparison with CP@GDY/DSPE-PEG, PFP and PBF only showed slight cytotoxicity towards 4T1 cells because of the hypoxia condition offering insufficient O_2 for CPs to kill cancer cells *via* PDT. Nevertheless, CP@GDY/DSPE-PEG could transform endogenous CO_2 into CO for continuous hypoxia cancer therapy.

The generated CO could interfere with mitochondrial respiration to induce cell apoptosis. To further explore the anticancer mechanism of CP@GDY/DSPE-PEG, the membrane potential of mitochondria was measured using a mitochondrial membrane potential probe, JC-1 (5,5′,6,6′-tetrachloro-1,1′,3,3′-tetraethyl benzimidazole carbonyl cyanine iodide). When JC-1 enters the cells and is distributed in the normal mitochondrial matrix with high membrane potential, it formed aggregation and emitted red fluorescence. For cells during the process of apoptosis, JC-1 presented decrement of the mitochondrial membrane potential, dispersed well, and emitted green fluorescence. As shown in Fig. 4c, negligible green fluorescence was observed in 4T1 cells treated with CP@GDY/DSPE-PEG

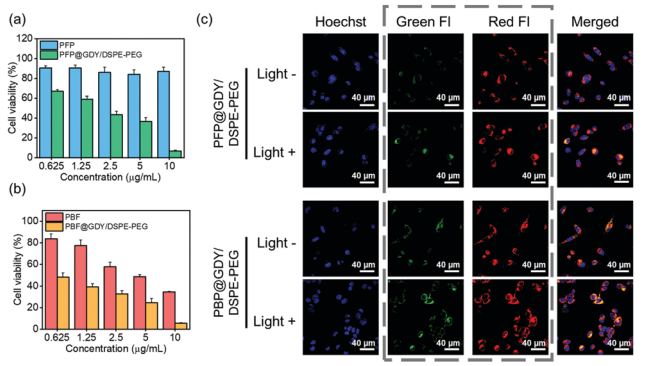

Fig. 4 MTT assay of 4T1 cells treated with PBF and PBF@GDY/DSPE-PEG (a), PFP and PFP@GDY/DSPE-PEG (b) in hypoxia condition. (c) Loss of mitochondrial membrane potential verified by JC-1 assay. The scale bar is 40 μm.

nanocatalyst without light irradiation. Under light irradiation, much intensive green fluorescence was observed, proving CP@GDY/DSPE-PEG induced cell apoptosis. The catalytic production of CO interferes with the normal physiological metabolism of mitochondria in the cell, showing a decreased mitochondrial membrane potential.

Conclusions

In conclusion, this work provides new CPs/GDY nanocatalysts to *in situ* reduce endogenous CO_2 to CO for hypoxia cancer therapy. The nanocatalysts were constructed through an assembly of CPs with GDY, which could photocatalyze CO_2 into CO at a rate of 23 μmol h^{-1} $gmat^{-1}$ for PFP@GDY/DSPE-PEG and 31 μmol h^{-1} $gmat^{-1}$ for PBF@GDY/DSPE-PEG under hypoxia condition, respectively. The catalytically generated CO inside the cells induces the loss of mitochondrial potential, and the ATP level was also affected in 4T1 cells, leading to cancer cell apoptosis. This work diversifies the research field of gas therapeutics, especially hypoxic tumor treatments.

Conflicts of interest

There are no conflicts to declare.

Acknowledgements

This study was financially supported by the National Natural Science Foundation of China (No. 21373243, 21473220).

Notes and references

1 Q. Y. Jia, Z. Y. Zhao, K. Liang, F. C. Nan, J. Wang, J. C. Wang and P. F. Wang, Recent Advances and Prospects of Carbon Dots in Cancer Nanotheranostics, *Mater. Chem. Front.*, 2019, **53**, 2241–2249.

2 Y. Y. Jiang, J. G. Huang, C. Xu and K. Y. Pu, Activatable Polymer Nanoagonist for Second Nearinfrared Photothermal Immunotherapy of Cancer, *Nat. Commun.*, 2021, **21**, 742.

3 Y. Zhang, C. Xu, X. L. Yang and K. Y. Pu, Photoactivatable Protherapeutic Nanomedicine for Cancer, *Adv. Mater.*, 2017, **32**, 2002661.

4 S. S. He, Y. Y. Jiang, J. C. Li and K. Y. Pu, Semiconducting Polycomplex Nanoparticles for Photothermal Ferrotherapy of Cancer, *Adv. Mater.*, 2020, **59**, 10633–10638.

5 J. Liu, B. Chen and J. J. Zhang, Preparation of pH-Responsive Doxorubicin Nanocapsules by Combining High-gravity Antisolvent Precipitation with *In situ* Polymerization for Intracellular Anticancer Drug Delivery, *Chem. Res. Chin. Univ.*, 2020, **36**, 927–933.

6 M. Q. Hao, B. B. Chen, X. Y. Zhao, N. N. Zhao and F. J. Xu, Organic/inorganic Nanocomposites for Cancer Immunotherapy, *Mater. Chem. Front.*, 2020, **4**, 2571–2609.

7 M. Z. Zou, W. L. Liu, H. S. Chen, X. F. Bai, F. Gao, J. J. Ye, H. Cheng and X. Z. Zhang, Advances in Nanomaterials for Treatment of Hypoxic Tumor, *Natl. Sci. Rev.*, 2020, **8**, 1–17.

8 H. Tian, Z. Y. Luo, L. L. Liu, M. B. Zheng, Z. Chen, A. Q. Ma, R. J. Liang, Z. Q. Han, C. Y. Lu and L. T. Cai, Cancer Cell Membrane-Biomimetic Oxygen Nanocarrier for Breaking Hypoxia-Induced Chemoresistance, *Adv. Funct. Mater.*, 2017, **27**, 1703197.

9 J. K. Fu, T. Li, Y. C. Zhu and Y. Q. Hao, Ultrasound-Activated Oxygen and ROS Generation Nanosystem Systematically Modulates Tumor Microenvironment and Sensitizes Sonodynamic Therapy for Hypoxic Solid Tumors, *Adv. Funct. Mater.*, 2019, **29**, 1906195.

10 W. L. Liu, T. Liu, M. Z. Zou, W. Y. Yu, C. X. Li, Z. Y. He, M. K. Zhang, M. D. Liu, Z. H. Li, J. Feng and X. Z. Zhang, Aggressive Man-Made Red Blood Cells for Hypoxia Resistant Photodynamic Therapy, *Adv. Mater.*, 2018, **30**, 1802006.

11 Q. Y. Jia, J. C. Ge, W. M. Liu, X. L. Zheng, S. Q. Chen, Y. M. Wen, H. Y. Zhang, P. F. Wang and A. Magnetofluorescent, Carbon Dot Assembly as an Acidic H_2O_2-Driven Oxygenerator to Regulate Tumor Hypoxia for Simultaneous Bimodal Imaging and Enhanced Photodynamic Therapy, *Adv. Mater.*, 2018, **30**, 1706090.

12 J. N. Moloney and T. G. Cotter, ROS Signalling in the Biology of Vancer, *Semin. Cell Dev. Biol.*, 2018, **80**, 50–64.

13 I. I. C. Chio and D. A. Tuveson, ROS in Cancer: the Burning Question, *Trends Mol. Med.*, 2017, **23**, 411–429.

14 S. B. Wang, C. Zhang, J. J. Ye, M. Z. Zou, C. J. Liu and X. C. Zhang, Near-Infrared Light Responsive Nanoreactor for Simultaneous Tumor Photothermal Therapy and Carbon Monoxide-Mediated Anti-Inflammation, *ACS Cent. Sci.*, 2020, **6**, 555–565.

15 J. Sun, X. T. Cai, C. J. Wang, K. Du, W. J. Chen, F. D. Feng and S. Wang, Cascade Reactions by Nitric Oxide and Hydrogen Radical for Anti-Hypoxia Photodynamic Therapy Using an Activatable Photosensitizer, *J. Am. Chem. Soc.*, 2021, **143**, 868–878.

16 P. Y. Zhang, H. Y. Huang, S. Banerjee, G. J. Clarkson, C. Ge, P. Imberti and P. J. Sadler, Nucleus-Targeted Organoiridium-Albumin Conjugate for Photodynamic Cancer Therapy, *Angew. Chem., Int. Ed.*, 2019, **58**, 2350–2354.

17 N. W. N. Simelane, C. A. Kruger and H. Abrahamse, Photodynamic Diagnosis and Photodynamic Therapy of Colorectal Cancer *in vitro* and *in vivo*, *RSC Adv.*, 2020, **10**, 41560–41576.

18 L. Y. Jiang, H. T. Bai, L. B. Liu, F. T. Lv, X. Q. Ren and S. Wang, Luminescent, Oxygen-Supplying, Hemoglobin-Linked Conjugated Polymer Nanoparticles for Photodynamic Therapy, *Angew. Chem., Int. Ed.*, 2019, **58**, 10660–10665.

19 Y. Zhou, W. Q. Yu, J. Cao and H. L. Gao, Harnessing Carbon Monoxide-Releasing Platforms for Cancer Therapy, *Biomaterials*, 2020, **255**, 120193.

20 B. S. Zuckerbraun, B. Y. Chin, M. Bilban, J. Costa d'Avila, J. Rao, T. R. Billiar and L. E. Otterbein, Carbon Monoxide Signals *via* Inhibition of Cytochrome *C* Oxidase and

Generation of Mitochondrial Reactive Oxygen Species, *FASEB J.*, 2007, **21**, 1099–1106.

21 J. Fang, R. Islam, W. Islam, H. Z. Yin, V. Subr, T. Etrych, K. Ulbrich and H. Maeda, Augmentation of EPR Effect and Efficacy of Anticancer Nanomedicine by Carbon Monoxide Generating Agents, *Pharmaceutics*, 2019, **11**, 343.

22 Y. J. Li, J. J. Dang, Q. J. Liang and L. C. Yin, Carbon monoxide (CO)-Strengthened Cooperative Bioreductive Anti-Tumor Therapy *via* Mitochondrial Exhaustion and Hypoxia Induction, *Biomaterials*, 2019, **209**, 138–151.

23 P. C. Kunz, H. Meyer, J. Barthel, S. Sollazzo, A. M. Schmidt and C. Janiak, Metal Carbonyls Supported on Iron Oxide Nanoparticles to Trigger the CO-Gasotransmitter Release by Magnetic Heating, *Chem. Commun.*, 2013, **49**, 4896–4898.

24 I. Kim, E. H. Han, W. Y. Bang, J. Ryu, J. Y. Min, H. C. Nam, W. H. Park, Y. H. Chung and E. Lee, Supramolecular Carbon Monoxide-Releasing Peptide Hydrogel Patch, *Adv. Funct. Mater.*, 2018, **28**, 1803051.

25 X. Y. Ji, L. K. Cruz, Z. X. Pan, V. Chittavong and B. H. Wang, pH-Sensitive Metal-Free Carbon Monoxide Prodrugs with Tunable and Predictable Release Rates, *Chem. Commun.*, 2017, **53**, 9628–9631.

26 X. X. Yao, P. Yan, Z. K. Jin, Q. Jiang, R. R. Guo, R. H. Xie, Q. J. He and W. L. Yang, Multifunctional Nanoplatform for Photoacoustic Imaging-Guided Combined Therapy Enhanced by CO Induced Ferroptosis, *Biomaterials*, 2019, **197**, 268–283.

27 S. Pillarisett, S. Mayaa, S. Sathianarayananb and R. Jayakumara, Tunable pH and Redox-Responsive Drug Release from Curcumin Conjugated γ-Polyglutamic Acid Nanoparticles in Cancer Microenvironment, *Colloids Surf., B*, 2017, **159**, 809–819.

28 Z. L. Li, W. Lu, S. C. Jia, H. X. Yuang, H. Y. Liang and L. H. Gao, Design and Application of Conjugated Polymer Nanomaterials for Detection and Inactivation of Pathogenic Microbes, *ACS Appl. Bio Mater.*, 2021, **4**, 370–386.

29 H. Zhao, J. W. Xu, K. Peng, X. C. Fu, E. D. Zhang, F. T. Lv, L. B. Liu, N. Zhang, Y. L. Wang, S. Wang and Q. Gu, Supramolecular Nanofibers for Encapsulation and in situ Differentiation of Neural Stem Cells, *Adv. Healthcare Mater.*, 2020, **9**, e1901295.

30 Z. L. Li, H. T. Bai, S. C. Jia, H. X. Yuan, J. H. Gao and H. Y. Liang, Design of Functional Polymer Nanomaterials for Antimicrobial Therapy and Combatting Resistance, *Mater. Chem. Front.*, 2021, **5**, 1236–1252.

31 C. L. Zhu, L. B. Liu, Q. Yang, F. T. Lv and S. Wang, Water-Soluble Conjugated Polymers for Imaging, Diagnosis, and Therapy, *Chem. Rev.*, 2012, **112**, 4687–4735.

32 H. J. Zhang, Y. C. Liang, H. Zhao, R. L. Qi, Z. Chen, H. X. Yuan, H. Y. Liang and L. Wang, Dual-Mode Antibacterial Conjugated Polymer Nanoparticles for Photothermal and Photodynamic Therapy, *Macromol. Biosci.*, 2020, **2**, 1900301.

33 X. C. Fu, H. T. Bai, F. T. Lyu, L. B. Liu and S. Wang, Conjugated Polymer Nanomaterials for Phototherapy of Cancer, *Chem. Res. Chin. Univ.*, 2020, **36**, 237–242.

34 Y. R. Xue, B. L. Huang, Y. P. Yi, Y. Guo, Z. C. Zuo, Y. J. Li, Z. Y. Jia, H. B. Liu and Y. L. Li, Anchoring Zero Valence Single Atoms of Nickel and Iron on Graphdiyne for Hydrogen Evolution, *Nat. Commun.*, 2018, **9**, 1460.

35 Z. C. Zuo, D. Wang, J. Zhang, F. S. Lu and Y. L. Li, Synthesis and Applications of Graphdiyne-Based Metal-Free Catalysts, *Adv. Mater.*, 2019, **31**, 1803762.

36 G. D. Shi, Z. X. Fan, L. L. Du, X. L. Fu, C. M. Dong, W. Xie, D. B. Zhao, M. Wang and M. J. Yuan, *In Situ* Construction of Graphdiyne/CuS Heterostructures for Efficient Hydrogen Evolution Reaction, *Mater. Chem. Front.*, 2019, **3**, 821–828.